CAMBRIDGE
UNIVERSITY PRESS

RESEARCH ARTICLE

Precise positioning in a robotized laser-cutting machine allowed by a three-V-shaped-groove kinematic coupling: a feasibility study

Carlo De Benedictis [iD] and Carlo Ferraresi [iD]

Department of Mechanical and Aerospace Engineering, Politecnico di Torino, Turin, Italy
Corresponding author: Carlo De Benedictis; Email: carlo.debenedictis@polito.it

Abstract

Devices known as kinematic couplings offer accurate, repeatable, and stiff connections between two parts. They are characterized by point contacts and enable great repeatability with errors less than 1 micron, in contrast to conventional coupling systems like alignment pins or those based on elastic deformation. In this study, a robotized laser-cutting machine is equipped with a three-groove kinematic coupling design to increase the precision of workpiece placement. Given the application's requirements, a preliminary design of the coupling is defined. An analytical approach is provided for calculating stresses and deflections at the locations where balls and grooves make contact, and it is then utilized to calculate positioning errors caused by the mechanical structure's elastic deformation under various loading conditions. The outcomes of the simulations are finally discussed and highlight the efficacy of the solution tested.

1. Introduction

High-precision couplings are necessary when two parts must be positioned relatively with accuracy. This is particularly common in automation industry or in environments where robots interact with surrounding elements. In this framework, coupling design can be critical to further improve the precision achieved by the robot. Moreover, this design also has an impact on the architecture and control of the robot, that, in order to work properly, should be able to correct those uncertainties related to the accuracy of the coupling, if requested by the application. In many scenarios, it is relevant to ensure the correct repeatability of the mechanical connection, that is the possibility to take apart and put back together the elements of the coupling. The accuracy of this connection must also be ensured for many cycles, unlike structural joints that are not supposed to be disassembled with continuity. In the following, a general description of the main coupling designs is presented.

Surface contacts represent the simplest design, in which two elements are connected through relatively flat interfaces. Among the several methods available to locate relatively two components, alignment pins surely represent the simplest solution [1]. In those conditions that require pressure mount between the pin and the hole, elastic deformation of the connection elements is necessary [2−4], resulting in over-determined couplings with redundant constraints. This is the case for pressure joints, wedges, guides, and grooves connections, that require an initial wear-in phase to reach the desired level of repeatability. By considering coupling devices based on surface contact, to achieve high precision in the relative positioning of two parts, strict tolerances in the manufacturing of the connection pieces are required. In some conditions, these tolerances could result stricter than the actual accuracy required by the coupling itself.

Designs shown above, based on surface contacts, generally constraint three degrees of freedom (DoFs) and achieve average repeatability (about 1 micron). On the other hand, quasi-kinematic and kinematic couplings allow for higher precision and repeatability. In particular, quasi-kinematic design is based on line contacts, hence it constrains two DoFs. For instance, a quasi-kinematic coupling [5, 6] is obtained through the connection between a convex element and a concave surface (groove) obtained on the second element of the coupling, which results in several arcs of contact. Compared to traditional surface contacts, the reduction to line contacts limits the load capacity of such designs; however, higher repeatability is allowed (about 0.5 micron) [7].

Kinematic couplings are static, precision-machined contacts that can enable high accuracy and repeatability in the relative positioning between two parts [8−11]. They are made in a way that the number of connections between two solid models corresponds to the number of limited DoF. In general, repeatable connections between two elements are obtained through six contact areas, which correspond theoretically to six points. Kinematic couplings can be selected for those applications in which engagements are routinely separated but, at the same time, high repeatability and accuracy must be achieved. When properly designed, these couplings are deterministic, hence the performance should be predictable just as maintenance requirements. In general, the weight of the component or forces provided by selected actuators and springs provide the nesting force. To keep the integrity of the coupling elements after many cycles, the design and manufacturing of those devices have to be performed carefully and with strict tolerances [12−14]. In particular, bad design can lead to failure due to fractures initiated in those points where stress is locally very high. Moreover, in theoretical point contact, no lubrication can be ensured between the two connecting elements. For these reasons, corrosion-resistant materials as ceramic are necessary for heavy applications where high loads and high-cycle are expected [15]. Despite the additional effort in the design of such couplings, repeatability can be very large, with errors lower than 1 micron even for steel-based connections [10].

In this work, the application of kinematic coupling design to a robotized laser-cutting machine is shown. In particular, a solution based on a three-V-shaped-groove coupling is chosen and designed with the aim of improving the precision of workpieces' positioning allowed by the machine, which has been originally dependent on a traditional "mushroom-socket" coupling with low repeatability. This work has been focused on the evaluation of the efficacy and feasibility of the solution proposed, and it has been carried out only at theoretical level and supported by simulations. A method used to evaluate the effect of deformations on the overall accuracy is presented, with a focus on load balancing that allows for further improving the accuracy of the system for most of the expected loading conditions. A preliminary discussion of this topic has already been published in a previous work from the authors [16], of which the current paper represents an extended version. In the following section, the structure of the laser-cutting machine is outlined and the implementation of the kinematic coupling in the machine design is discussed. Then, a preliminary design and the analysis of the three-groove kinematic coupling are carried out, in order to assess the stresses and deflections that affect the resulting positioning accuracy. The results of the simulations are finally shown and discussed.

2. Implementation of the Kinematic Coupling in the Laser-Cutting Machine Design

This work is a case-study type. In particular, it has been developed as part of a project run by a company that ranks among the world's leaders in laser-cutting and welding fields [17]. Aim of the study is to evaluate the feasibility of kinematic coupling for the precise positioning of workpieces in a robotized laser-cutting machine designed by the company. Objectives of this work are the mechanical design of the coupling and the assessment of its accuracy, given the target precision of 0.02 mm required by the application. Figure 1a shows the CAD assembly of the machine.

The system is made up of two separate modules that are placed next to one another. Each module is positioned on a cart (see Fig. 1b) that is pulled by a gear motor mounted on a linear guide. This translation occurs to move the module between the loading station, where workpieces are positioned on
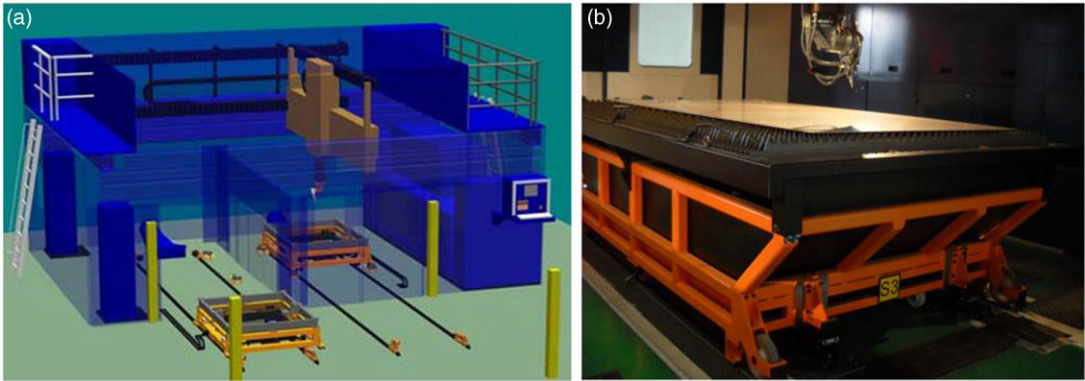
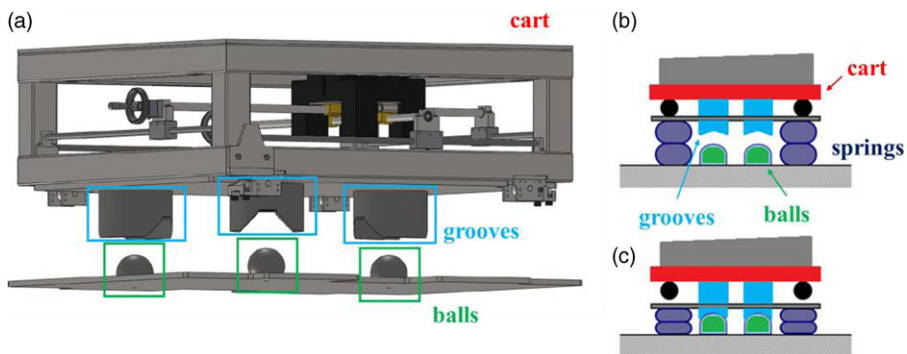**Figure 1.** *(a) The CAD model of the laser-cutting machine; (b) one of the modules of the machine.*

Figure 2. *The implementation of the three-groove kinematic coupling: (a) the model of the cart, sketched without springs and linear guides, along with coupling elements; sketches of disengaged (b) and engaged (c) configurations [16].*

the cart and the actual machining station. Height-adjustable wheels are installed at the four corners of the structure to provide mobility within the working space. In the original configuration, the accuracy of the positioning of the cart in the working area depended on a traditional "mushroom-socket" type of coupling, which limits the repeatability of the connection as well as its precision, due to the effects of wear on the coupling elements. This phenomenon depends on the number of cycles, and it is difficult to predict its effect on the accuracy of the system. Moreover, any error in the positioning of the cart directly affected the precision of the manufacturing on the workpiece. For this reason, a solution based on a kinematic coupling has been investigated.

Among the several designs available, the one considering three V-shaped grooves and three spheres/balls, in a triangular configuration, has been adopted (see Fig. 2a).

Other shapes as the Kelvin Clamp coupling have been preliminary considered but discarded in favor of the three-groove coupling solution from James Clerk Maxwell due to the symmetric configuration, which also reduces the costs of manufacturing. Both designs have been formerly developed in the early 1800 [10]. The introduction of a dedicated positioning system based on kinematic coupling allows for improved precision with respect to the original configuration. Indeed, once in the machining station, the cart can be decoupled from the linear guide and the vertical motion required to achieve workpiece's ultimate positioning is permitted. To provide the necessary level of accuracy, the final placement occurs only on the coupling parts. Two industrial air springs placed between the rails and the plane below are inflated and deflated to regulate the vertical movement (as shown in Fig. 2b–c). Side linear guides (not shown in Fig. 2a) are necessary since the air spring's elasticity does not ensure a straight vertical motion.
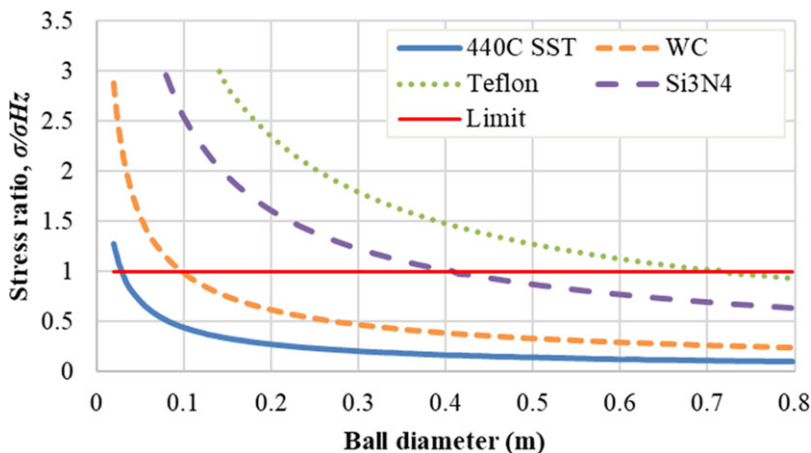
Figure 3. *Comparison between the different materials tested for several ball diameters.*

3. Design of the Three-Groove Kinematic Coupling

Three balls and three V-shaped grooves positioned at the vertices of an equilateral triangle serve as the final connection structure [18, 19]. The ball element is a 100 mm diameter spherical shell with a base at 3/4 of the height overall. A threaded hole is bored into its flat surface to attach it to the base. This configuration requires that the spheres are stationary while the grooves are part of the cart that translates vertically (see Fig. 2b–c). Each groove is a cylinder with a 200 mm diameter and a 127.5 mm height. For each groove-ball couple, the contact surfaces are cut with an angle of 90° between them on one side of the groove.

The dimensioning of the components requires an appropriate choice of the materials. In particular, the behavior of a hardened stainless steel (440C SST, 200 GPa elastic modulus, 0.28 Poisson ratio), tungsten carbide (WC, 683 GPa elastic modulus, 0.24 Poisson ratio), Teflon (PTFE, 1.32 GPa elastic modulus, 0.46 Poisson ratio), and a ceramic (Si3N4, 240 GPa elastic modulus, 0.25 Poisson ratio) have been compared. In this preliminary analysis, the following data were considered to characterize the system:

- diameter of the coupling, depending on the available surface below the cart: 0.8 m;
- weight of the cart: 3000 N;
- weight of the workpiece: 4500 N.

The static analysis yielded the results shown in Fig. 3.

For this preliminary evaluation, the point of application of the load was considered coincident to the centroid of the coupling, hence all the elements of the coupling were subjected to the same stress. For each material and ball diameter, the ratio between the contact pressure and the allowable Hertzian stress σHz, namely the contact (Hertzian) stress ratio $\sigma/\sigma Hz$, has been estimated. For metals, the allowable Hertzian stress has been set to 1.5 times the ultimate tensile strength [20], whereas for the other materials, the ultimate compressive strength has been considered. In order to achieve low-stress ratio (below 50%), as well as to have smaller dimensions and lower production costs, 440C stainless steel was chosen. The final diameter of 100 mm led to 45% of stress ratio, as shown by data presented in Fig. 3.

Calculating the stresses and deflections at the contact, which have an impact on the positioning error permitted by the kinematic coupling, is necessary for the coupling's design. The key phases of this technique are described below, and more details can be found in the literature [18]. It begins with knowledge of the following information:
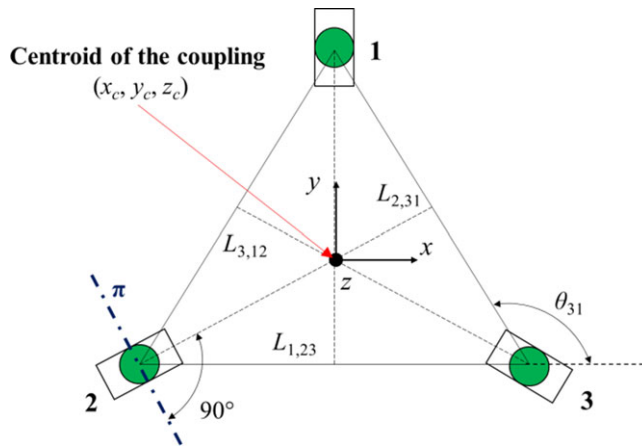
Figure 4. *Equilateral triangle shape of the three-groove kinematic coupling.*

- the size of the ball elements and radii of curvature of the grooves;
- the locations of the contact points between the spheres and the grooves;
- the contact forces' orientation;
- the coordinates of the points at which the preload forces are applied and their magnitude;
- the external load magnitude and its point of application;
- the elastic modulus and Poisson coefficient of each material considered.

The normals to the planes holding the contact force vectors for each ball must bisect the internal angles between two consecutive sides of the coupling triangle in order to satisfy the theoretical stability criterion for exact three-groove kinematic couplings [10]. In the illustration of Fig. 4, for example, the normal to the plane π should split in half the angle between the sides joining the couples 12 and 23.

Being defined by the geometry of the system, as well as the physical parameters listed above, the calculation of the six contact forces F_{bi} is obtained by Eq. (1), hence by performing the static analysis of the system. This calculation requires the knowledge of the external force $\boldsymbol{F}_e$ and moments $\boldsymbol{M}_e$ vectors acting on the coupling:

$$\sum \boldsymbol{F}_e = \boldsymbol{0}, \quad \sum \boldsymbol{M}_e = \boldsymbol{0} \quad \longrightarrow \quad F_{b_i}, \quad (i = 1 \ldots 6) \tag{1}$$

The estimation of stresses and deflections depends on the geometry of the contact area. For this particular kinematic coupling design, the contact region is shaped as an ellipse (see Fig. 5) with semi-major axis $R_{\max}$ and semi-minor axis $R_{\max}$. To perform their calculation, the equivalent elastic modulus E_e and the equivalent radius R_e must be known. They are given by Eq. (2):

$$E_e = \frac{1}{\frac{(1-v_g{}^2)}{E_g} + \frac{(1-v_b{}^2)}{E_b}}, \quad R_e = \frac{1}{\frac{1}{R_{g\max}} + \frac{1}{R_{g\min}} + \frac{1}{R_{b\max}} + \frac{1}{R_{b\min}}} \tag{2}$$

where $R_{b\max}$ and $R_{b\min}$ have the same value, $R_{g\max}$ is infinite (i.e., $1/R_{g\max} = 0$), and $R_{g\min}$ is negative. As shown in Eq. (2), elastic modulus and Poisson coefficients are assigned for both coupling elements. Finally, the semi-major axis and semi-minor axis can be estimated as shown in Eq. (3), given the force F acting on the ball-groove coupling:

$$R_{\max} = \alpha \left(\frac{3FR_e}{2E_e} \right)^{1/3}, \quad R_{\min} = \beta \left(\frac{3FR_e}{2E_e} \right)^{1/3} \tag{3}$$

where α and β are functions of the geometric factor $\cos\theta$ and can be both approximated as polynomial expressions. For this problem, $\cos\theta$ reduces to $R_e/|R_{g\min}|$ [18]. Finally, the Hertzian contact stress σ and
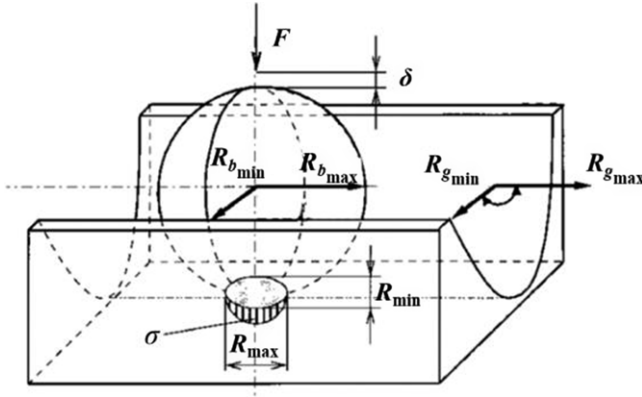
Figure 5. *Detail of ball-groove contact for a generic geometry of the groove [16].*

deflection δ are calculated for each ball-groove couple with Eq. (4):

$$\sigma = \frac{3F}{2\pi R_{max} R_{min}}, \quad \delta = \lambda \left(\frac{2F^2}{3R_e E_e{}^2} \right)^{1/3} \tag{4}$$

where λ is a function with similar meaning to α and β in Eq. (3).

The positioning errors in the kinematic coupling may be estimated once the contact stresses and deflections have been found. The weighted average of ball deflections obtained by using Eq. (4) may be used to determine the deviations $\delta_{\xi c}$ ($\xi = x, y, z$) of the centroid of the coupling triangle in the scenario where the spheres' relative positioning is not changing noticeably. Rotation errors ε_x and ε_y are then calculated, starting from the segments' lengths L and angles θ, see Fig. 4 for reference. This methodology yields the results shown in Eqs. (5) and (6), under small rotation angles assumption:

$$\varepsilon_x = \frac{\delta_{z1}}{L_{1,23}} \cos \theta_{23} + \frac{\delta_{z2}}{L_{2,31}} \cos \theta_{31} + \frac{\delta_{z2}}{L_{3,12}} \cos \theta_{12} \tag{5}$$

$$\varepsilon_y = \frac{\delta_{z1}}{L_{1,23}} \sin \theta_{23} + \frac{\delta_{z2}}{L_{2,31}} \sin \theta_{31} + \frac{\delta_{z2}}{L_{3,12}} \sin \theta_{12} \tag{6}$$

The average of the rotations about z, with regard to the coupling's centroid, computed for each ball, is used to obtain the rotation error around the z-axis as shown in Eq. (7):

$$\varepsilon_z = \frac{\varepsilon_{z1} + \varepsilon_{z2} + \varepsilon_{z3}}{3} \tag{7}$$

The relation shown in Eq. (8) may be used to calculate the translation errors δ_ξ ($\xi = x, y, z$) at any location around the coupling once the rotation errors ε_x, ε_y, and ε_z (in radians) have been calculated.

$$\begin{bmatrix} \delta_x \\ \delta_y \\ \delta_z \\ 1 \end{bmatrix} = \begin{bmatrix} 1 & -\varepsilon_z & \varepsilon_y & \delta_{xc} \\ \varepsilon_z & 1 & -\varepsilon_x & \delta_{yc} \\ -\varepsilon_y & \varepsilon_x & 1 & \delta_{zc} \\ 0 & 0 & 0 & 1 \end{bmatrix} \cdot \begin{bmatrix} x - x_c \\ y - y_c \\ z - z_c \\ 1 \end{bmatrix} - \begin{bmatrix} x - x_c \\ y - y_c \\ z - z_c \\ 0 \end{bmatrix} \tag{8}$$

4. Estimation of Positioning Accuracy Allowed by the Kinematic Coupling

In this section, the analyses carried out to assess the positioning accuracy of the coupling are presented, and their results are discussed. In particular, the methodology shown in the Section 3 was applied to
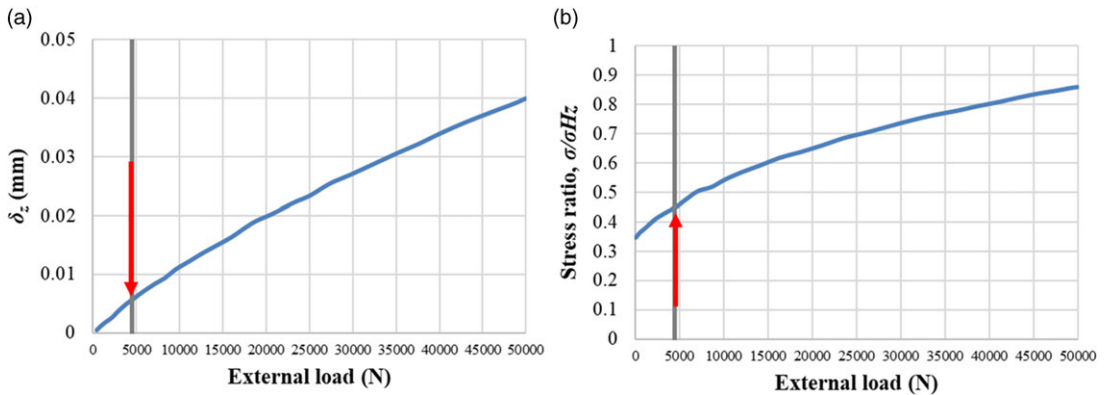
Figure 6. *Vertical deflection (a) and Hertzian stress ratio (b) obtained when increasing external load is applied at the center of gravity of the cart. Arrows directed to the point corresponding to cart's payload.*

estimate position and orientation errors for different loading conditions. The study represents a preliminary investigation aimed at implementing such a coupling system in a practical scenario, that is the laser-cutting machine presented in Section 2; therefore, all the analyses have been performed only at simulation level. To achieve realistic results, however, parameters from the actual machine have been considered when available, otherwise they have been estimated (as the overall expected mass of the coupling elements). The parameters considered for the simulations are listed below:

- cart's payload: 450 kg;
- overall mass of the cart, coupling elements included: 300 kg;
- loading area on the cart: 1.1 m × 1.1 m;
- target positioning accuracy: 0.02 mm.

For each simulation, errors δ_ξ and ε_ξ ($\xi = x, y, z$) were estimated, as well as the Hertzian stress ratio $\sigma/\sigma Hz$.

The initial analysis looked at system deformations by taking into account objects of various weights put on the cart and placed at its center of gravity. This investigation was required to determine if the target repeatability could be obtained even under the most extreme load. Figure 6 shows the findings of this investigation. The displacement at the center of gravity is entirely vertical, since the cart and coupling centroids are coincident, and equivalent to about 0.006 mm when using a weight of 4500 N, which represents the anticipated payload. The stress ratio $\sigma/\sigma Hz$ for this condition results equal to about 45%.

To emphasize the impact of load eccentricity on the overall accuracy, the location of the external load was then altered. In this study, it was shifted along the y axis (see Fig. 4 for reference), as allowed by the symmetry of the kinematic coupling triangle. Figure 7 shows the results of this analysis. Ball element 1 has a larger maximum $\sigma/\sigma Hz$ than that found for balls 2 and 3. The higher stress ratio is attained when the weight is placed directly on the ball 1 (58%), but when the midpoint between balls 2 and 3 is taken into account, stress ratio is lowered to 34%. The trends for 2 and 3 are overlapping, as seen in Fig. 7b, due to the symmetry.

According to Fig. 7a, the total deformation along the z-axis varies by the order of one thousandth of a millimeter. However, it should be noted that the deformation varies locally on the spheres. By examining each ball separately, the greatest vertical deformation at ball 1 is calculated to be 0.0114 mm, which is in any case less than the limit of 0.02 mm. It is also confirmed the impact of rotation about the x-axis. Indeed, the rotation error ε_x decreases as the external load approaches the coupling's center of gravity. When the force is applied directly to ball 1, the maximum ε_x of 1.9e−5 is used, yielding an overall displacement of 0.0143 mm, hence still acceptable for this application.
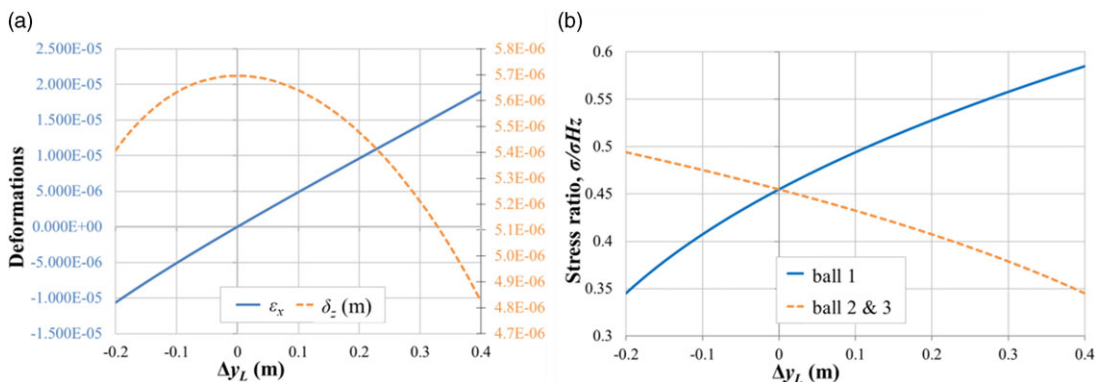
Figure 7. *Rotation and vertical deflections (a) and Hertzian stress ratios (b) for several locations of the external load on the cart. Δy_L represents the deviation from the centroid of the coupling and of the cart.*
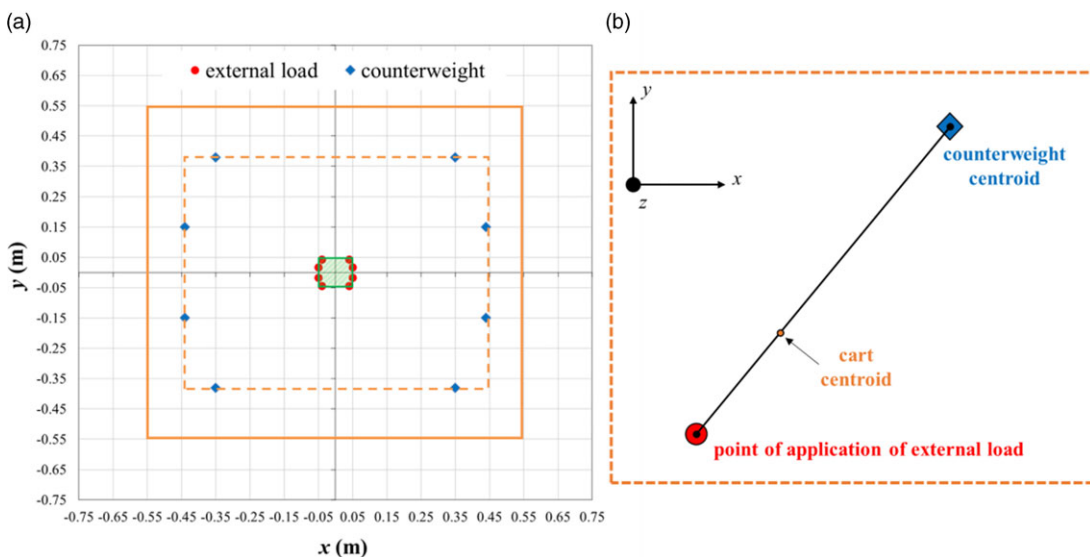

Figure 8. *(a) Space of action of the counterweight: thick line denotes the cart, and dashed line denotes the area within the counterweight has to be contained in order to avoid obstructions with surrounding elements. The green-dot area represents the space available to the external load's point of application that still results in perfect balancing. (b) The relative positioning of external load, cart, and counterweight centroids in an explanatory configuration.*

Although being still lower than 0.02 mm, positioning error results significantly affected by eccentric location of the external load. This aspect is critical for the robustness and reliability of the solution, hence the effect of load balancing on the system has been evaluated in the final analysis. At the risk of increased bulkiness and weight of the system, it is expected to improve the precision of the coupling for most of the loading conditions. By balancing the moments exerted on the system made up of the cart and the coupling elements, it was possible to estimate the counterweight's field of action, leading to the outcome shown in Fig. 8. The counterweight, which has plant view measurements of 0.34 m × 0.2 m, is a 50 kg cast iron industrial weight.

The size and weight of the chosen counterweight determine how large is the green region visible in Fig. 8a. By making the deformations on the spheres consistent, balancing compensates the rotational
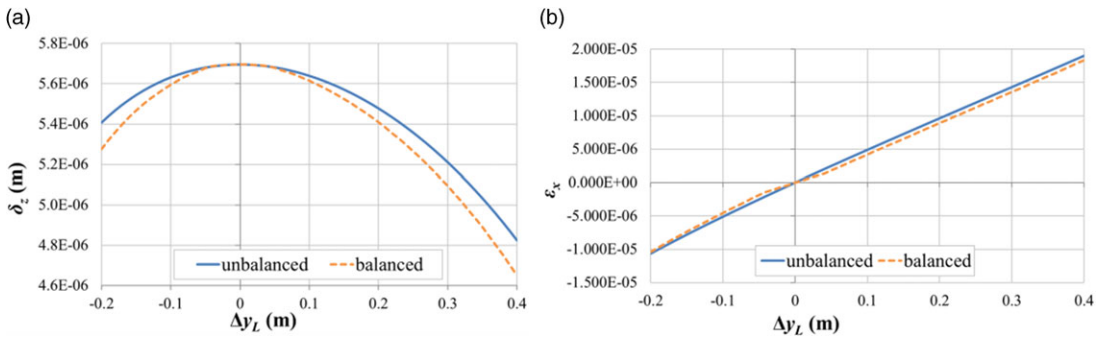
(a)

(b)

Figure 9. *Vertical deflection (a) and rotation error about the x axis (b) for unbalanced and balanced conditions. Δy_L represents the deviation from the centroid of the coupling and of the cart.*

errors that would otherwise be worsened by shifting away from the coupling's centroid. Figure 9 shows the resulting deflections and rotation errors obtained for the unbalanced and balanced conditions. The deformations δ_z and ε_x are always lower than that obtained for the unbalanced case: even by considering the largest errors shown in Fig. 9b, the maximum accuracy error results equal to 0.0138 mm.

5. Conclusion

This paper deals with the implementation of a kinematic coupling in a robotized laser-cutting machine aimed at improving the accuracy and repeatability of workpieces' positioning. A three-groove coupling architecture has been adopted for this purpose, whose feasibility and efficacy have been studied at theoretical level. This work has proved that such a solution can enable improved precision, which is relevant for robotic applications that include industrial automation, collaborative environments, and so on. Enhanced accuracy can possibly influence control design too, since positioning errors can be partially compensated by the coupling design itself. Nonetheless, it should be noted that similar solutions are not viable in any application and require a study of deformations and stresses at contacts between coupling elements.

The process for estimating the positioning error was outlined, starting with the system's physical properties and the implementation of Hertz's theory. The investigation took into account the machine's usual loading circumstances, which include unbalanced weights put on the cart in use. The coupling systems have shown to ensure positioning accuracy with errors smaller than 0.02 mm at each location, as needed by the application, under every test condition. The study has been carried out at simulation level; therefore, the practical implementation will be objective of future works. However, the results presented in this work support the adoption of such a system to improve the overall performance of the machine.

In addition to the lack of experimental data, other limitations of the current study are related to the phenomena that have been neglected for the sake of simplicity. In particular, friction between the contact surfaces affects the repeatability of the coupling. Ceramic materials allow for minimized coefficients of friction, in addition to improved performance in terms of corrosion. Therefore, they might represent a good solution in terms of increased repeatability. On the other hand, coupling elements manufactured in steel can improve mechanical performance and lower the costs of manufacturing.

Given the difficulty in modeling friction effects, experimental tests in a real scenario will be necessary to assess the exact repeatability allowed by the kinematic coupling, for instance on realistic scale model. The same approach might be necessary to assess the effect of surface texture and lubricants on the accuracy and repeatability of this solution.

References

[1] R. R. Vallance, C. Morgan and A. H. Slocum, "Precisely positioning pallets in multi-station assembly systems," *Precis. Eng.* **28**(2), 218–231 (2004). doi: 10.1016/j.precisioneng.2002.11.003.

[2] A. H. Slocum. *Precision Machine Design* (Prentice-Hall, Inc, Englewood Cliffs, NJ, 1992).

[3] M. Ciavarella, A. Baldini, J. R. Barber and A. Strozzi, "Reduced dependence on loading parameters in almost conforming contacts," *Int. J. Mech. Sci.* **48**(9), 917–925 (2006). doi: 10.1016/j.ijmecsci.2006.03.016.

[4] N. J. van de Berg, T. L. De Jong, D. J. Van Gerwen, J. Dankelman and J. J. Van Den Dobbelsteen, "The influence of tip shape on bending force during needle insertion," *Sci. Rep.* **7**(1), 40477 (2017). doi: 10.1038/srep40477.

[5] D. Guamàn-Lozada, H. Ahuett-Garza, A. P. Castro-Martin, J. Ruiz-Carrizal, M. F. Márquez-Alderete, J. G. Anaya-Aranda, T. R. Kurfess and E. G. de Castilla, "Design and testing of a positioning system based on a quasi kinematic guide and a clamp plate suspended by compliant straps for in-line metrology systems," *Manuf. Lett.* **24**, 19–22 (2020). doi: 10.1016/j.mfglet.2020.03.006.

[6] D. Zhang, P. Li, W. Xu, Z. Li, G. Jin and J. Zhang, "A strain-free semi-kinematic mount for ultra-precision optical systems," *Opt. Lasers Eng.* **134**, 106287 (2020). doi: 10.1016/j.optlaseng.2020.106287.

[7] M. L. Culpepper, "Design of quasi-kinematic couplings," *Precis. Eng.* **28**(3), 338–357 (2004). doi: 10.1016/j.precisioneng.2002.12.001.

[8] L. C. Hale and A. H. Slocum, "Optimal design techniques for kinematic coupling," *Precis. Eng.* **25**(2), 114–127 (2001). doi: 10.1016/S0141-6359(00)00066-0.

[9] M. L. Culpepper, M. V. Kartik and C. DiBiasio, "Design of integrated eccentric mechanisms and exact constraint fixtures for micron-level repeatability and accuracy," *Precis. Eng.* **29**(1), 65–80 (2005). doi: 10.1016/j.precisioneng.2004.05.007.

[10] A. H. Slocum, "Kinematic couplings: A review of design principles and applications," *Int. J. Mach. Tools Manuf.* **50**(4), 310–327 (2010). doi: 10.1016/j.ijmachtools.2009.10.006.

[11] E. Budak, A. Matsubara, A. Donmez and J. Munoa, "Mechanical interfaces in machine tools," *CIRP Ann.* **71**(2), 647–670 (2022). doi: 10.1016/j.cirp.2022.05.005.

[12] A. H. Slocum, "Kinematic couplings for precision fixturing—Part I: Formulation of design parameters," *Precis. Eng.* **10**(2), 85–91 (1988). doi: 10.1016/0141-6359(88)90005-0.

[13] A. H. Slocum, L. Muller and D. Braunstein, Flexural mount kinematic couplings and method, 2005, US Patent No. US5678944A.

[14] R. W. Penny and A. J. Hart, "Precision assembly of additively manufactured components using integral kinematic couplings," *Precis. Eng.* **60**, 104–115 (2019). doi: 10.1016/j.precisioneng.2019.04.011.

[15] A. H. Slocum and A. Domnez, "Kinematic couplings for precision fixturing —part 2: Experimental determination of repeatability and stiffness," *Precis. Eng.* **10**(3), 115–122 (1988). doi: 10.1016/0141-6359(88)90029-3.

[16] C. De Benedictis and C. Ferraresi, "Study of a three-groove kinematic coupling for precise positioning in a robotized laser-cutting machine," *Adv. Service Ind. Robot.* **120**, 264–271 (2022). doi: 10.1007/978-3-031-04870-8_31.

[17] Prima Industrie S.p.A. Homepage. https://www.primaindustrie.com/it, last accessed 2022/01/31.

[18] A. H. Slocum, "Design of three-groove kinematic couplings," *Precis. Eng.* **14**(2), 67–76 (1992). doi: 10.1016/0141-6359(92)90051-W.

[19] L. C. Hale, "Testing the limiting coefficient of friction with an adjustable 3-V kinematic coupling," *Precis. Eng.* **64**, 200–209 (2020). doi: 10.1016/j.precisioneng.2020.04.003.

[20] R. J. Roark and W. C. Young. *Formulas for Stress and Strain*, 5th edition, McGraw-Hill Book Co., New York, (1975).